Environmental Science and Policy 124 (2021) 235–246

Contents lists available at ScienceDirect

Environmental Science and Policy

journal homepage: www.elsevier.com/locate/envsci

The GOS^{4}M Knowledge Hub: A web-based effectiveness evaluation platform in support of the Minamata Convention on Mercury

Francesco De Simone *, Francesco D'Amore, Mariantonia Bencardino, Francesco Carbone, Ian M. Hedgecock, Francesca Sprovieri, Sergio Cinnirella, Nicola Pirrone

CNR-Institute of Atmospheric Pollution Research, Division of Rende, UNICAL Polifuzionale, 87036 Rende (CS), Italy

ARTICLE INFO

Keywords:
Minamata Convention on Mercury
Mercury pollution
Mercury emission reduction
Policy scenarios
Decision support system

ABSTRACT

The Minamata Convention on Mercury was established to reduce the pressure on the environment caused by mercury by significantly reducing its emissions from anthropogenic activities. However, knowledge gaps still exist concerning emission inventories, emission factors and their integration in modelling frameworks. In addition, tools to facilitate communication between decision-makers and research groups providing measurement and modelling data are still scarce. This work presents the GOS^{4}M Knowledge Hub, a public web application that provides an interactive and user friendly experience to access state-of-the-art modelling tools and data available in the literature. The Knowledge Hub currently integrates a Chemical Transport Model emulator, HERMES, coupled with a biogeochemical model, although it has been designed to house and deploy any number of different modelling components. Using the integrated dashboard, non-experts can perturb mercury releases from different anthropogenic emission sectors, simulating, for example, the application of Best Available Technologies, and then visualise in real-time the short- and long-term effects of the consequent reductions within a source-receptor framework. The dashboard also furnishes an estimate of the statistical significance of the changes in the model results. The analysis of a set of anthropogenic Hg emission reduction scenarios shows how an internationally coordinated effort would be necessary to achieve significant policy goals. It is important to note that the GOS^{4}M Knowledge Hub yields the analysis presented here in a matter of seconds, compared to the days or weeks required by traditional modelling tools.

1. Introduction

The Minamata Convention on Mercury (MCM) (http://www.mercuryconvention.org/), which came into effect in August 2017, was established to reduce mercury (Hg) contamination by anthropogenic activities. During its implementation through the Conference of Parties, discussion focused on initialising the operation of the Specific International Programme and providing guidance to the Global Environment Facility on strategies, policies, programme priorities and eligibility for access to and utilisation of financial resources (UN-Environment, 2019).

A fundamental activity of the MCM was outlined by the ad hoc technical expert group for effectiveness evaluation, which proposed a framework for the implementation assessment, and the need for standardised global monitoring arrangements. This expert group identified a list of gaps to be filled, in order to harmonise emission inventories, redefine emission factors and integrate modelling frameworks. In addition, the expert group for effectiveness evaluation raised policy-relevant questions that have been brought to the attention of the scientific community, and that need to be addressed by further research. Decision-makers require information on changes of Hg levels in the environment, in biota, and vulnerable populations, so that they can be attributed to the implementation of the Convention. They also require an assessment of the actions taken in terms of the changes in Hg supply and usage, and the resulting variation in Hg emission and release to the environment. In this context, the integration of modelling capabilities to assess changes in global mercury levels, within and across environmental media, will aid the effectiveness evaluation and the implementation of the Convention, if they are made easily available through information technologies. Definitely, there is a need for a change in paradigm to bring environmental data (observed, analysed, modelled)

Abbreviations: GOS^{4}M-KH, GOS^{4}M Knowledge Hub; MCM, Minamata Convention on Mercury; CTM, chemical transport model; BGCM, biogeochemical model; ES, earth system; Hg_{anthr}, Hg emitted from anthropogenic activities; Hg_{ES}, Hg cycling within ES compartments.

* Corresponding author.
E-mail address: francesco.desimone@iia.cnr.it (F. De Simone).

https://doi.org/10.1016/j.envsci.2021.06.021
Received 19 March 2021; Received in revised form 16 June 2021; Accepted 24 June 2021
Available online 2 July 2021

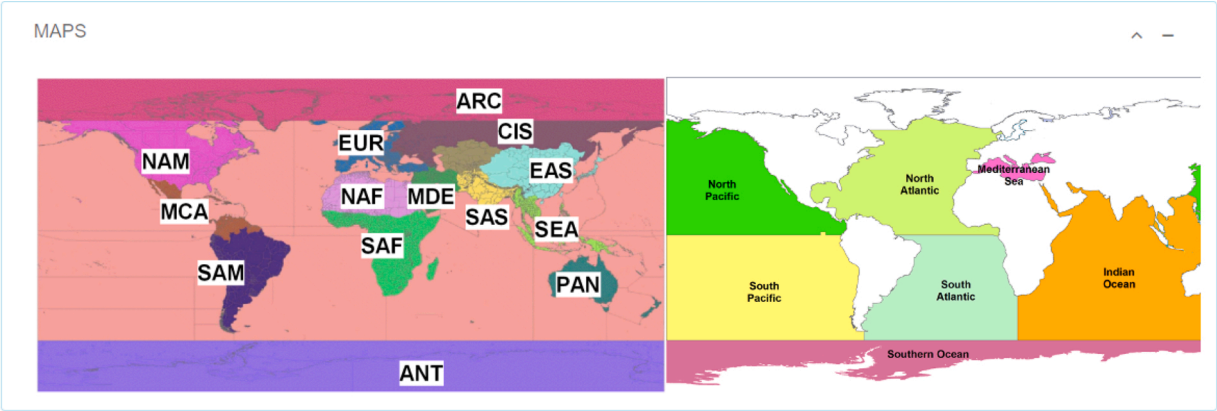

Fig. 1. Left panel: definition of the source regions used. NAM (North America), EUR (Europe), SAS (South Asia), EAS (East Asia), SEA (South East Asia), PAN (Australia), NAF (North Equatorial Africa), SAF (South Equatorial Africa), MDE (Middle East Asia), MCA (Central America), SAM (South America), CIS (Central Asia), ARC (Arctic, above 66° N). Right panel: Ocean Basin definition; NAT (North Atlantic), SAT (South Atlantic), NAP (North Pacific), SAP (South Pacific), MED (Mediterranean Sea) and SOC (Southern Ocean). Note that SOC and ANT are, respectively, the ocean and the Antarctic continent below 60° S. Receptor regions include both ocean basins and source regions.

to the decision-maker, in the form of knowledge, rather than raw results (Talia, 2015).

The current workflow for sharing scientific knowledge with policy makers is rather complex and it can take a significant amount of time for the latest scientific discoveries to be included in the materials available to support policy decisions.

This workflow starts with anthropogenic mercury (Hg_{anth}) emissions estimates (AMAP/UNEP, 2013; Muntean et al., 2018; Zhang et al., 2016b), which are then required to be linked to Hg deposition fields.

Currently, only complex models, referred to as chemical transport models (CTMs), specifically designed to study the atmospheric cycle of Hg, are capable of simulating in detail the fate of atmospheric Hg_{anthr} from its release points to the final receptors. A number of Hg-CTMs has been developed over the last decades, and these include, among others, GLEMOS (Travnikov and Ilyin, 2009; Travnikov et al., 2009), GEM-MACH-Hg (Durnford et al., 2012; Kos et al., 2013; Dastoor et al., 2015), GEOS-CHEM (Holmes et al., 2010; Amos et al., 2012; Song et al., 2015; Horowitz et al., 2017; Zhang et al., 2019), and ECHMERIT (Jung et al., 2009; De Simone et al., 2014). See Travnikov et al. (2017) for a detailed description of these state-of-the-art Hg-CTMs, which have all been systematically used to study the impacts of natural processes and anthropogenic activities on the Hg atmospheric cycle (De Simone et al., 2015, 2017a; Saiz-Lopez et al., 2018; Zhou et al., 2021; Fraser et al., 2018).

Hg has a biogeochemical cycle (Amos et al., 2013), therefore the temporal scope of a CTM simulation is generally limited, due to approximations of the exchange processes between the atmosphere and the other compartments, in particular the oceans (Kawai et al., 2020). The integration, or the coupling, of the CTMs with oceanic models (Kawai et al., 2020; Zhang et al., 2019) or biogeochemical models (BGCMs) (Amos et al., 2013, 2014; Selin, 2014) allows for a more detailed modelling of Hg exchange between environmental compartments within the earth system (Hg_{ES}), and the compartments' relative Hg burdens, with simulations being able to be extended for centuries.

These models require dedicated hardware on which to run, and many input and output manipulation steps are indispensable to perform simulations, analyse, and present the results in a meaningful way for third parties. Numerous runs are necessary to obtain Hg deposition fields based on current and perturbed emissions for short periods of a few years. Many further runs are also required to provide an evaluation of the uncertainty and, given the necessity of a certain level of expertise, these models are far from being user-friendly and interactive tools, which may be directly used by policy makers.

Only after all the pre-processing, model execution, and post-processing steps, are the scientific results finally shared with policy makers or other stakeholders by standard publications or other means, including web applications for customised assessments.

A recent paper describes a statistical emulator built around the ECHMERIT CTM (Jung et al., 2009; De Simone et al., 2014), referenced HERMES by authors (De Simone et al., 2020). The model can provide in real-time the short-term effects (nominally one-year) on anthropogenic Hg_{anth} deposition fluxes resulting from Hg_{anth} emissions perturbations, within a source-receptor framework.

HERMES makes a number of assumptions, for the purpose of statistical tractability (e.g., by including only the Hg_{anthr} in the model) and therefore its scope is limited in time and application to short-term analyses. Although atmospheric deposition can be considered a good indicator, or proxy, for the level of organic mercury (MeHg) in water and biota (Chen et al., 2019; Giang and Selin, 2015; Zhang et al., 2016a), the re-emissions from soils and oceans of previously deposited Hg_{anth} (also referred to as legacy emissions) are important sources of Hg to the atmosphere, that need to be considered explicitly, since these processes can be modulated by climate changes, that on a longer time-scale, can play a role in determining Hg deposition fluxes (Giang and Selin, 2015; Schartup et al., 2019; Schaefer et al., 2020).

HERMES has therefore been coupled to a BGCM, adapted from Selin (2014), to explicitly simulate the cycling of Hg between Earth System compartments (hereafter Hg_{ES}), for a further 34 years, nonetheless retaining the real-time experience for users.

Current (and future) computational modules are included in a web application under the GOS^{4}M Knowledge Hub (GOS^{4}M-KH) https://sdi.iia.cnr.it (see Section 2.3 for details on the GOS^{4}M-KH developed as single component of the Spatial Data Infrastructure (SDI) (D'Amore et al., 2012), the Data Catalogue and the analysis tools). The GOS^{4}M-KH presented in this study was developed as an effort to bring the latest scientific results and modelling tools to policy makers and stakeholders, allowing the easy assessment of Hg_{anthr} emission reduction scenarios and their real-time evaluation.

2. Materials and methods

In this section all the components of the GOS^{4}M-KH, including the modelling modules, the technological infrastructure, as well as the web interface are described.

2.1. HERMES CTM emulator

Hg_{anthr} emissions perturbation is emulated using HERMES, a

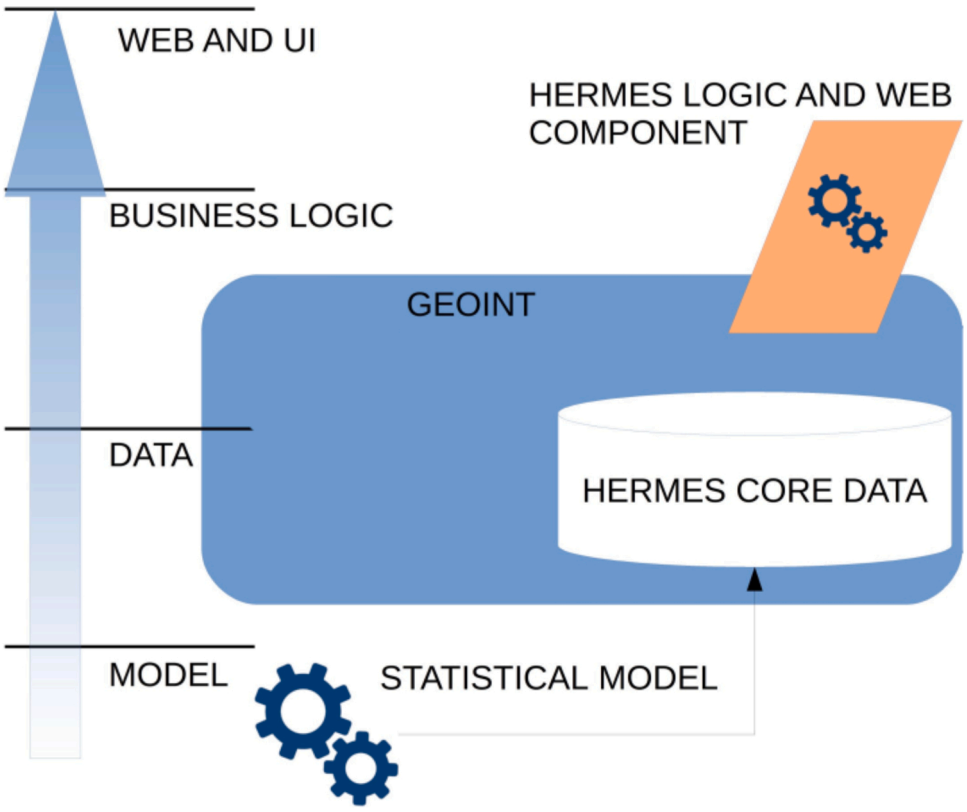

Fig. 2. The layers that define the web application: the statistical model developed off line is stored in the DATA LAYER. The BUSINESS LOGIC LAYER layer provides processes and procedures to manage user interactions triggered in the WEB and User Interface layer.

statistical CTM emulator (De Simone et al., 2020). The emulator uses the results of a pre-designed set of different source-receptor runs performed using the global Hg-CTM model ECHMERIT (Jung et al., 2009; De Simone et al., 2014). HERMES allows for the emulation of the Hg-CTM model ECHMERIT results regarding Hg deposition over receptor regions following perturbation of the Hg_{anthr} emissions in one or more source regions. It is possible to both reduce Hg_{anthr} emissions, and to modify the Hg/Hg^{II} ratio, to simulate the implementation of flue gas treatment technologies.

The source and receptor regions, as defined in the HTAPv2 experiment (http://www.htap.org/) are shown in Fig. 1.

The HERMES core is represented by the following polynomial equation:

$$DEP_{r,s}^{HERMES} = A_{s,r}^{Spec} * (100 - INPUT_s^{Red}) + INPUT_s^{Spec} * B_{s,r}^{Spec} * (100 - INPUT_s^{Red}) \quad (1)$$

which permits the calculation of the new deposition $DEP_{r,s}^{HERMES}$, in the receptor region r resulting from the change in Hg_{anthr}, due to either emission reduction ($INPUT_s^{Red}$), or change of emission speciation ($INPUT_s^{Spec}$) in the source region s.

$INPUT_s^{Spec}$ represents the ratio between $Hg_{(g)}^0$ (0 = 100%) and Hg^R (1 = 100%) specified by the user to perturb Hg_{anthr} emissions. $A_{s,r}^{Spec}$ and $B_{s,r}^{Spec}$ are the coefficients of the linear regression relating speciation alteration and deposition, whereas $INPUT_s^{Red}$ is the Hg_{anthr} emission reduction in the source region s as a percentage (0–100%), as specified by the user.

The new deposition value, $DEP_{r,s}^{HERMES}$, is then compared to the relative bounds at the 95% confidence level, and an indication is reported if it falls outside the bounds.

HERMES is designed to allow the emulation of Hg_{anthr} deposition change over one or more receptors, nominally one year after the Hg_{anthr} emission perturbation in one or more source regions.

2.2. Details of biogeochemical model

To estimate the longer term effects of changing Hg_{anth} emissions, we integrated a BGCM, adapted from Selin (2014) that makes use of the short term Hg deposition change from the HERMES emulator to calculate the cycling of Hg_{ES} over the following 34 years, to gain an indication of the potential impacts, particularly regarding the deposition of Hg_{ES} over oceans and the Hg_{ES} burden within ocean.

The BGCM is a simple six-box model based on the present day Hg_{CE} cycle and reservoirs, where all fluxes are assumed to be first-order processes. The model simulation is initialised with current data, regarding the Hg_{ES} burden and fluxes (Selin, 2014), except for the new Hg_{anth} emission value, that is passed by HERMES. Moreover, the BGCM makes use of the Hg_{anthr} deposition flux change over seas and land to recalculate the relative rates of deposition of Hg over these compartments, i.e., the first order transfer coefficients $k_{atmosphere,j}$ from reservoir *atmosphere* to reservoir j = *sea*, *land*, defined as

$$F_{atmosphere,j} = k_{atmosphere,j} \times M_{atmosphere} \quad (2)$$

where $F_{atmosphere,j}$ is the flux from reservoir *atmosphere* to reservoir j = *sea*, *land* and $M_{atmosphere}$ is the burden of Hg_{ES} in the atmosphere.

Potential changes in the mobilisation of Hg_{ES} from reservoirs due to meteorology, climate forcing, and alteration in the intensities and patterns of biomass burning, will be included in future versions of the model.

The model is implemented in python (https://www.python.org/) and is called by the web platform at each user interaction, as explained below.

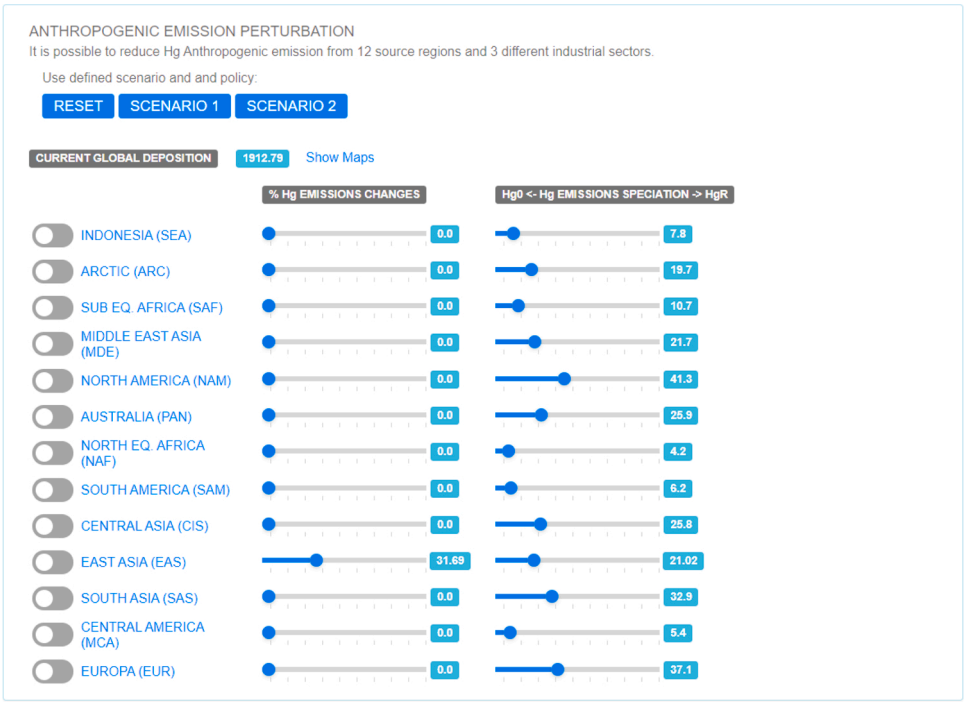

Fig. 3. Screenshot of the *Regional input* widget to change Hg_{anth} emissions from different source regions.

2.3. The GOS^{4}M-KH Dashboard: backend

The two core elements described above, the HERMES atmospheric CTM emulator and the BGCM, are included in a web application available at www.gos4m.org/kh.

The web application was designed using the architecture described in Fig. 2: the statistical model (MODEL LAYER) of HERMES is created offline, stored in a database (DATA LAYER) and triggered at each user interaction. In the DATA LAYER, the matrices $A_{s,r}^{Spec}$ and $B_{s,r}^{Spec}$ used in Eq. (1), are stored and then provided to the BUSINESS LOGIC LAYER when needed.

The BUSINESS LOGIC LAYER provides the procedures to retrieve the HERMES model from the DATA LAYER and manage its data structures. The BUSINESS LOGIC LAYER uses the HERMES model in order to simulate different emission scenarios responding to user interactions on the Web User Interface. This User Interface is designed to be as responsive as possible, and to enhance its user friendliness.

The Web Dashboard is able to include third-party components, not developed by the core team working on HERMES: the biogeochemical model, discussed in Section 2.2, is plugged in the framework in order to improve the scenarios provided to HERMES's users. The biogeochemical model uses the output of the HERMES core model as input. As can be seen in Fig. 2, the design is such that third-party components can be plugged in the BUSINESS LOGIC LAYER, where corresponding data structures are designed and developed for each software component to be included.

From a technological point of view, the software layers in Fig. 2 are developed using Java Enterprise and related third-party libraries. Data is stored in a PostgreSQL Data Base Management System (DBMS) (https://www.postgresql.org/), wrapped using MyBatis (https://mybatis.org/), an Object Relational Mapping (ORM) tool able to define porting between DATA LAYER and BUSINESS LOGIC LAYER. The BUSINESS LOGIC LAYER is developed using an Inversion of Control framework (IoC) in order to define a well containerised logic for each component.

The User Interface is developed using ZKoss (https://www.zkoss.org/), a Java library to develop fast and interactive web components. The final product is deployed in a *servlet container* able to host java objects (Tomcat 8.5.16). GOS^{4}M-KH, and the related web dashboard, is one of the components that makes up the Spatial Data Infrastructure (SDI) of the CNR-IIA (https://sdi.iia.cnr.it) designed to manage data and processes (D'Amore et al., 2012).

The entire web platform runs in a virtual machine hosted on the

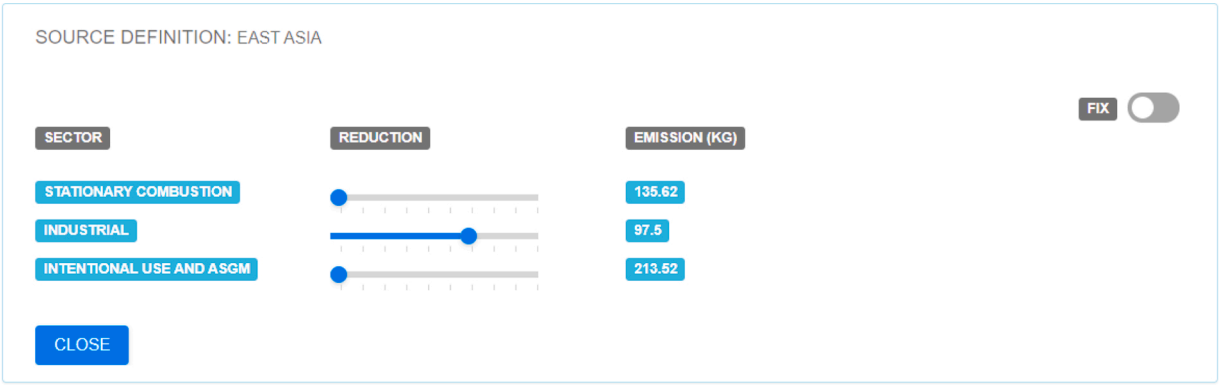

Fig. 4. Screenshot of the *Sector input* widget for Hg_{anth} emission sectors reduction for the selected source region.

institutional cloud infrastructure provided by the CNR as IaaS (Infrastructure as a Service).

2.4. The GOS^{4}M-KH Dashboard: front-end

The front-end of the GOS^{4}M-KH web application is designed to be as user-friendly as possible, using a series of separated widgets, dedicated to the different aspects addressed by the tool, in a sequence recalling the workflow from the emission perturbation to the intended final endpoint (s) to be evaluated. A number of cursors and buttons allow simple and intuitive interaction between the user and the tool(s), whereas a series of graphics and other elements illustrate in real-time the process results, which, differently, would take days or more using conventional modelling.

The first section (Fig. 3), is the *Regional Input* widget. In this area there are two sliders to perturb Hg_{antrh} emissions for each of the source regions. The first allows the user to reduce the emissions (in percentage terms), whereas the second adjusts the $Hg^0_{(g)}$ to Hg^R ratio. A switch to the left of the source region names allows Hg_{antrh} emissions to be increased rather than decreased.

Finally, a reset button allows the user to clear the Hg_{antrh} emission changes.

A second widget, that refers to the *Sector Input*, can be expanded by clicking on the name of the source region (Fig. 4), allowing the reduction of Hg_{anth} release from each of the three emission macro-sectors. In this case the user can cut the Hg_{anth} emissions in absolute terms (Mg), and the corresponding overall Hg_{anth} emission reduction and the speciation values in the *Regional input* widget, will change accordingly.

In the illustrated instance we decreased the Hg_{anth} INDUSTRIAL emission sector by 68% (corresponding to a new emission 97.5 Mg/y from 304.7 Mg/y), and the tool automatically accounted for the overall reduction of Hg_{anth} emissions in the regions (31.69%) and for the corresponding new $Hg^0_{(g)}$ to Hg^R ratio (21.02:88.98 in comparison to 20.6:89.4).

The *Atmospheric output* widget shows the list of terrestrial and oceanic receptor regions. When the Hg_{anth} emissions are changed using the sliders in either the *Regional input* or the *Sector input* widgets, the percentage change of Hg_{antrh} deposition over the receptor regions, is shown immediately. As explained, these results are to be considered as nominal annual changes, one year after the Hg_{anthr} emission perturbation. These boxes are normally blue, however they become green or red if the Hg_{anthr} deposition decreases or increases in a statistically significant manner (95% level of confidence), respectively. The global ocean cell summarises the total deposition change (as a percentage) over the oceanic receptors after one year, as calculated by HERMES, and after 10 years, as calculated by the BGCM, see below.

In the same widget, the results are shown graphically, reporting the Hg_{anthr} deposition in (Mg/y) in the new scenario compared to the current (Business as Usual) case, for each receptor region.

The widget that follows in the sequence shows the *Biogeochemical output*. As before, any user action applied to *Regional input* or *Sector input* widget triggers the execution of the CTM emulator, whose output provides the input for the BGCM, which in turn calculates the cycling of Hg_{ES} within the compartments of ES for the following 34 years. At the end of the process, which takes fractions of a second, effectively in real-time for the user, two plots illustrate the temporal evolution of two variables of interest, the Hg_{ES} deposition over all oceans (in Mg/y) and the Hg_{ES} burden within the intermediate ocean layer (in Mg) the for the same years. Both plots show the evolution of the relevant variable for three different scenarios: (a) Business as Usual (in black), Hg_{anth} emissions remain constant at today's levels, (b) Deep Green (in green), representing the case where the Hg_{anth} emissions drop to zero, and (c) the New Scenario, as calculated by the BGCM following the Hg_{anth} emission perturbation by the user.

Table 1
Hg_{anthr} emissions released by different sectors in each of the source regions. The asterisk indicates the source regions that are the six main emitters for the specific sector.

Source region	Sector emissions (Mg/y)		
	COMB	INDU	INTW
INDONESIA (SEA)	5.96	18.1	*50.64
ARCTIC (ARC)	0	5.9	0.1
SUB EQ. AFRICA (SAF)	*48.1	*37.13	*208.16
MIDDLE EAST ASIA (MDE)	1.26	13.37	6.35
NORTH AMERICA (NAM)	*45.13	14.78	7.93
AUSTRALIA (PAN)	2.47	13.88	0.49
NORTH EQ. AFRICA (NAF)	1.08	13.69	*56.88
SOUTH AMERICA (SAM)	1.3	*41.38	*155.5
CENTRAL ASIA (CIS)	*19.12	*57.13	35.51
EAST ASIA (EAS)	*135.62	*304.7	*213.52
SOUTH ASIA (SAS)	*66.03	*61.03	32.52
CENTRAL AMERICA (MCA)	3.71	21.87	*70.81
EUROPA (EUR)	*49.08	*39.29	15.85

3. Results

The use of the GOS^{4}M-KH as a useful tool to support policy decisions in accordance with the MCM is illustrated by a series of case studies of different Hg_{anthr} emission reduction scenarios presented in the following sections. Our purpose is to assess the extent of the short- and long-term effects of reducing the Hg_{anthr} emissions from a single macro-sector in the main emission regions.

3.1. Scientific background

In order to provide the context of the scientific process, which led to the development of the GOS^{4}M-KH, we summarise the key findings of previously published work, which are also useful in interpreting the results presented in the following sections.

In De Simone et al. (2016) we compared three Hg_{anthr} emission inventories (AMAP/UNEP, 2013; Muntean et al., 2014; Streets et al., 2009. An ensemble of ECHMERIT-CTM (Jung et al., 2009; De Simone et al., 2014) sensitivity runs was constructed by varying Hg_{anthr} emission inventory, Hg_{anthr} oxidation mechanism, and other relevant parameters. The analysis of the ensemble showed that the global distribution of Hg_{anthr} deposition is characterised by a notable variability over industrialised regions and remote areas. Moreover, the Arctic and Mediterranean seas appeared to be the basins where the Hg_{anthr} emission impact is proportionally the greatest.

In De Simone et al. (2017b) a regionally tagged version of ECHMERIT-CTM was used to simulate the fate of Hg_{anthr} in a set of sensitivity runs, in order to provide an estimate of the uncertainty associated with the source-receptor matrix of Hg_{anthr} deposition. In almost all receptors the Hg_{anthr} emissions, released from remote regions impacts on deposition more than domestic Hg_{anthr} emissions, at a 95% level of confidence. In general, the results clearly indicate that the uncertainty associated with Hg_{anthr} deposition for many source-receptors pair is so high that it is necessary that it be taken into consideration by policy makers.

These and other factors have convinced the authors of the need for a robust modelling tool that could be used by non-expert users in a real-time fashion. The underlying research has led to the development of the HERMES-CTM emulator (see (De Simone et al., 2020) and Section 2.1) and its integration in the GOS^{4}M-KH.

3.2. Scenario definition

The AMAP/UNEP 2010 global inventory, prepared for the UNEP 2013 Global Mercury Assessment AMAP/UNEP (2013), was used as input for scenario simulation in ECHMERIT. It provides global gridded mercury emissions for 2010 at 0.5° × 0.5° resolution. The inventory

Table 2
Hg_{anthr} emission reduction scenarios evaluated using HERMES.

Source region	Sector emissions (Mg/y)		
	COMB	INDU	INTW
INDONESIA (SEA)	5.96	18.1	*50.64
ARCTIC (ARC)	0	5.9	0.1
SUB EQ. AFRICA (SAF)	*48.1	*37.13	*208.16
MIDDLE EAST ASIA (MDE)	1.26	13.37	6.35
NORTH AMERICA (NAM)	*45.13	14.78	7.93
AUSTRALIA (PAN)	2.47	13.88	0.49
NORTH EQ. AFRICA (NAF)	1.08	13.69	*56.88
SOUTH AMERICA (SAM)	1.3	*41.38	*155.5
CENTRAL ASIA (CIS)	*19.12	*57.13	35.51
EAST ASIA (EAS)	*135.62	*304.7	*213.52
SOUTH ASIA (SAS)	*66.03	*61.03	32.52
CENTRAL AMERICA (MCA)	3.71	21.87	*70.81
EUROPA (EUR)	*49.08	*39.29	15.85

gives detailed emissions by industrial sectors that in this assessment have been grouped in macro-sectors. Stationary combustion, power and heating plants emissions have been grouped into the COMB macro-sector, stationary combustion for industry into INDU, Intentional-use/product, waste and artisanal gold-scale mining (ASGM) emissions into INTW.

Table 1 reports Hg_{anthr} emissions for each source region.

In order to test the web platform, 12 Hg_{anthr} emission reduction scenarios were assessed. The first 9 scenarios were built selecting the main 6 regional emitters for each sector and cutting the emissions by 10%, 20% and 50%. The remaining 3 scenarios were built by combining the main 6 regional source emitters for each sector and cutting the Hg_{anthr} emissions by 10%, 20% and 50%. The details of the tested scenarios are summarised in Table 2.

The widgets shown in Figs. 3 and 4 were used to implement the scenarios defined in Table 2, then the short-term effects on Hg_{anthr} deposition were analysed using the widget illustrated in Fig. 5. Long-term effects on Hg_{ES} deposition over global oceans and Hg_{ES} burden within the intermediate ocean layer were analysed using the widget reported in Fig. 6.

3.3. Short-term effects of policy scenarios

Table 3 reports, for each of the analysed scenario, the results of Hg_{anthr} deposition change, in percentage, over the land and ocean receptors.

The effects of the Hg_{anth} emission reduction in different scenarios on the resulting short-term deposition can be very different among the receptors. However, some general outcomes can be identified.

A reduction of any of the three sectors (INTW, INDU and COMB) alone of less than 50% (Scenarios S1, S2, S4, S5, S7 and S8) results in no significant deposition reduction over any receptor region.

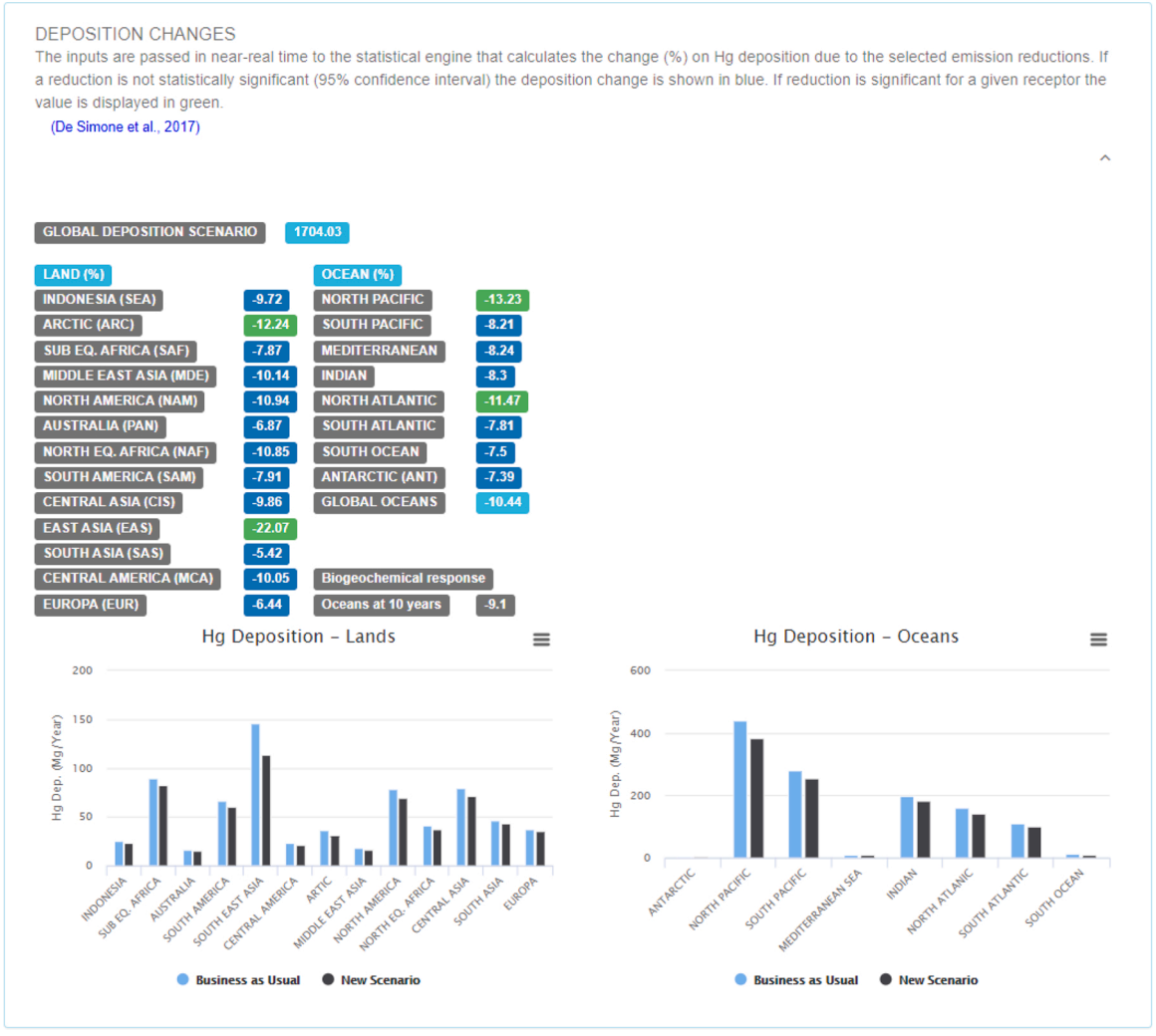

Fig. 5. Screenshot of the *Atmospheric output* widget, showing for each of the receptor regions the percentage change for the short term Hg_{anth} deposition (nominally one year) resulting from Hg_{anth} emission perturbation.

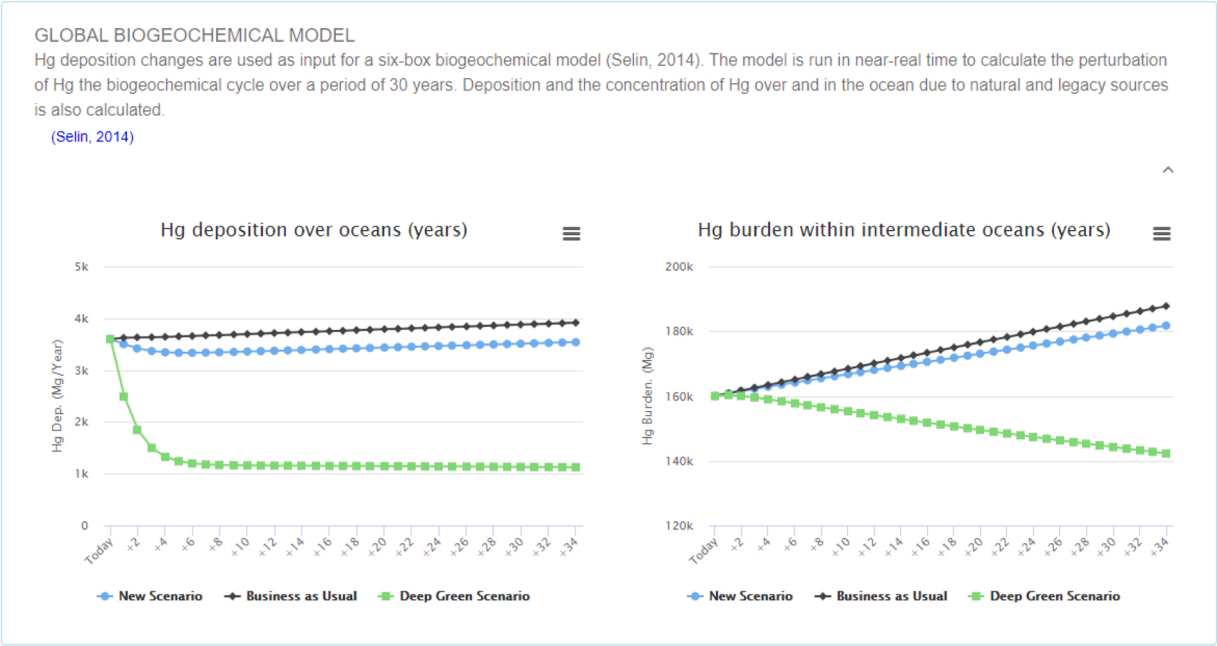

Fig. 6. Screenshot of the *Biogeochemical output* widget, which reports the temporal evolution trends of the Hg_{ES} deposition over all oceans (in Mg/y) and the Hg_{ES} burden within the intermediate ocean layer (in Mg) for more than 30 years in the future.

A reduction of INTW of 50% (Scenario S9) results in a significant deposition reduction over all ocean receptor regions and over almost all terrestrial receptor regions except the Antarctic, Central Asia, East Asia, Europe, North Eq. Africa and South Asia.

A reduction of INDU of 50% (Scenario S6) results in a significant deposition reduction only over the Arctic, Central Asia, East Asia, Middle East Asia, the North Atlantic and the Mediterranean Sea.

A reduction of COMB of 50% (Scenario S3) results in a significant deposition reduction over only 4 regions: Europe, the Arctic, the Mediterranean Sea and the North Atlantic.

When a reductions of 10% (Scenario S10) is applied to the top 6 emitters of the relevant sectors contemporaneously, no one receptor shows an advantage in terms of significant deposition change, whereas when the reduction is the 20% (Scenario S11), only the deposition reduction over Australia, South Asia, the Southern Ocean and the Antarctic is not significant. A reductions of 50% (Scenario S12) applied to the top 6 emitters leads to a significant deposition reduction over all receptor regions.

Fig. 7 summarises which regions benefit the most and least from the emission reductions in the scenarios.

For the Arctic, Mediterranean Sea and North Atlantic the Hg_{anth} short-term deposition decreases significantly in 5 out 9 scenarios. In particular these regions benefit from 50% Hg_{anth} emission reduction for each of the macro-sectors, COMB (*S*3), INDU (*S*6) and INTW (*S*9), and also for the 20% and 50% emission reduction from all macro-sectors (*S*11 and *S*12). The same applies to Middle East Asia and the North Pacific, with the exception of 50% reduction from COMB (*S*3). By contrast, Hg_{anth} short-term deposition over the Antarctic and South Asia is significant only in the *S*12 scenario. It is significant for South Equatorial Africa only in the *S*11 and *S*12 scenarios, whereas over the Southern Ocean and Australia the deposition reduction is significant only in the *S*9 and *S*12 scenarios. This range of significance, demonstrated by the policy scenarios in the different receptors, is due to the rather broad confidence interval of the Hg_{anth} deposition over some of the receptors, in particular those reported in the lower panel of Fig. 7 (for details, see De Simone et al. (2017b)).

Fig. 8 summarises the numbers of the receptor regions where the investigated policy scenarios lead to a significant decrease in Hg_{anth} short-term deposition, as calculated by CTM emulator module.

As noted previously, only a meaningful (at least 20%) and contemporaneous reduction of Hg_{anth} emissions of all the macro-sectors considered has a significant effect over most receptors globally (to 17 of 21 and to all 21 receptors for a reduction of 20% and 50%, respectively).

3.4. Long-term effects of policy scenarios

The BGCM module, integrated in the web application, was then exploited to evaluate the scenario being investigated in terms of long-term effects on Hg_{ES} deposition over oceans and Hg_{ES} burden within the intermediate ocean layer, the results of which are shown in Figs. 9 and 10 , respectively.

No one scenario associated with COMB and INDU macro-sector Hg_{anth} emissions produces significant changes in the BGCM indicators analysed, although the *S*6 scenario resembles the lower 95% CI limit of the current, Business as Usual, scenario. When considering the INTW macro-sector, only the scenario with a reduction of 50% led to a significant change in terms of both Hg_{ES} deposition over oceans and the Hg_{ES} burden within oceans. Also, when considering all macro-sectors, both the reduction of 20% and 50%, scenario *S*11 and *S*12, result in significant change.

4. Discussion

4.1. Challenge for policy implementation

The crucial role of the scientific community to inform policy makers is being demonstrated during the current (at time of writing) coronavirus pandemic, European Union, 2020 (https://ec.europa.eu/info/sites/info/files/research_and_innovation/contact/documents/factsheet_sharing-knowledge-informing-policy_lr.pdf). An efficient and timely cooperation between scientific community and policy makers and stakeholders may lead to enforce the legislation and evaluate its effectiveness over a given period of time. Science is generally focused on monitoring our ecosystems using state of the art methodologies and technologies, understanding chemical and physical processes and how

Table 3
Hg_{anthr} deposition changes, expressed as a percentage, over the land and ocean receptors for the scenarios evaluated with HERMES. Bold values indicate significant changes.

Scenario	ANT	ARC	CIS	EAS	EUR	SEA	MCA	MDE	NAF	NAM	PAN	SAF	SAM	SAS	IND	NAT	SAT	NPA	SPA	MED	STO
S1	−1.2	−2.1	−2.6	−2.3	−4.1	−1.8	−1.6	−1.8	−2.1	−2.7	−1.1	−1.6	−1.3	−4.0	−1.6	−2.1	−1.3	−1.8	−1.3	−3.1	−1.2
S2	−2.5	−4.2	−4.8	−4.6	−7.6	−3.6	−3.2	−3.7	−4.2	−5.5	−2.3	−3.4	−2.6	−7.3	−3.3	−4.2	−2.7	−3.7	−2.7	−6.0	−2.6
S3	−6.5	**−10.5**	−11.5	−11.6	**−18.1**	−8.9	−8.2	−9.2	−10.5	−14.0	−6.0	−8.6	−6.7	−17.1	−8.3	**−10.6**	−6.9	−9.4	−6.8	**−14.6**	−6.5
S4	−2.2	−3.1	−3.9	−3.9	−3.7	−2.6	−2.4	−2.7	−2.9	−2.5	−2.0	−2.3	−2.4	−3.9	−2.5	−2.8	−2.3	−3.0	−2.3	−3.3	−2.2
S5	−4.4	−6.2	−7.4	−7.8	−6.9	−5.2	−4.9	−5.3	−5.8	−5.1	−4.0	−4.7	−4.8	−7.1	−5.0	−5.6	−4.6	−6.0	−4.6	−6.3	−4.5
S6	−11.2	**−15.5**	**−18.0**	**−19.5**	−16.4	−13.0	−12.4	**−13.4**	−14.4	−12.8	−10.1	−11.8	−12.1	−16.7	−12.4	**−14.1**	−11.6	**−15.1**	−11.7	**−15.3**	−11.3
S7	−5.2	−3.2	−2.5	−3.1	−1.8	−4.0	−4.3	−3.2	−3.6	−3.1	−4.5	−4.8	−5.2	−1.9	−4.6	−3.7	−5.1	−3.9	−5.0	−2.6	−5.2
S8	−10.4	−6.5	−5.1	−6.2	−3.6	−8.1	−8.7	−6.4	−7.3	−6.1	−9.0	−9.7	−10.3	−3.8	−9.2	−7.5	−10.2	−7.8	−9.9	−5.2	−10.3
S9	−26.0	**−16.1**	−12.6	−15.6	−9.1	**−20.5**	**−22.1**	**−16.1**	−18.3	**−15.4**	**−22.5**	**−24.2**	**−25.6**	−9.4	**−22.9**	**−18.6**	**−25.5**	**−19.5**	**−24.8**	**−13.2**	**−25.8**
S10	−9.6	−9.5	−10.1	−9.9	−10.3	−9.7	−9.6	−8.7	−9.7	−9.7	−8.5	−9.7	−9.8	−10.5	−9.7	−9.7	−9.7	−9.8	−9.6	−10.0	−9.6
S11	−19.3	**−19.1**	**−19.9**	**−19.8**	**−20.2**	**−19.5**	**−19.4**	**−17.4**	**−19.5**	**−19.6**	−17.1	**−19.5**	**−19.5**	−20.3	**−19.5**	**−19.6**	**−19.4**	**−19.6**	**−19.3**	**−19.7**	−19.2
S12	**−48.2**	**−47.6**	**−49.1**	**−49.5**	**−49.6**	**−49.0**	**−48.9**	**−43.5**	**−48.8**	**−49.1**	**−42.8**	**−48.9**	**−48.9**	**−49.6**	**−48.7**	**−49.0**	**−48.5**	**−49.0**	**−48.3**	**−49.0**	**−48.2**

they may affect the uncertainty associated to our measurements, validate CTMs against measurements, and disseminating major findings in scientific peer-reviewed literature. Information Technology can help in the preparation of tools that "translate" scientific findings into user-friendly interfaces. The GOS^{4}M-KH is implementing this approach by providing a tool to analyse long-term (up to decades) Hg deposition scenarios with changing anthropogenic emission regimes. The overarching goal is that monitoring data sets, multi-compartment model runs, geospatial data analysis and graphical rendering that are usually research tools, are brought to end-users for customised assessments.

In the policy making context such as that related to a Conference of Parties (COP), Representatives of Countries, NGOs, and Stakeholders are called to take decisions that should ensure the achievement of policy target(s) that may (will) likely have significant implications on various economic sectors (i.e., industrial and manufacturing sectors) at their country or regional scale. Therefore, there is a strong need to make available user-oriented knowledge hubs or systems that allow to analyse possible links between causes (emission sectors or emission regions) and effects (i.e., human exposure to Hg bioaccumulated in the food chain) and identify cost-effective strategies that may allow decision makers to reduce the risk associated to these Hg exposure patterns. The GOS^{4}M-KH is an example of a user-friendly platform that may allow decision makers to evaluate different options for answering specific policy relevant questions (i.e., what is the reduction of Hg bioaccumulated in fish to a given reduction of anthropogenic emissions to the atmosphere?) and choose the most cost-effective strategy that has been proved to be more suitable for a given country or region.

The challenge in designing and running the GOS^{4}M-KH lies also in the need for collaborative effort. The GOS^{4}M Flagship has a well-established Governance and all Members are major experts in the various fields of mercury science. Scientists that manage monitoring networks, run regional or global mercury multi-compartment models, analyse chemical and physical processes affecting Hg dynamics, are part of this community oriented to support policy implementation. It is well known that the scientific community has supported since the beginning (2002) the preparation of the Minamata Convention on Mercury and is engaged in assisting all interested parties in its implementation. The possibility to use well validated platforms, which integrate monitoring data with state of the art multi-compartment models and policy scenario analysis, may contribute to ensure that policy decisions will be based on well consolidated scientific evidence.

4.2. *Current implementation and future development*

The Hg_{anthr} tool and the scenario analyses presented and discussed here, show the potential use of robust and validated scientific modelling tools by non-expert end-users.

To overcome the temporal scope of the previous published HERMES-CTM emulator (De Simone et al., 2020), it has been coupled with a BGCM, adapted from Selin (2014), which is called by the web application following the execution of CTM module. At this stage of development, however, the BGCM considers a single ocean compartment. Therefore, currently it is possible to analyse only the overall effects on oceans, without the possibility to assess the impact on single basins, or fisheries. In the future development, a more detailed BGCM will be included, considering explicitly the same ocean basins defined for the CTM emulator, in order to extend the temporal scope of the scenario assessment within a source-receptor framework.

The improvement of the application (De Simone et al., 2020) introduces the possibility to act on a single macro-sector, as defined in AMAP/UNEP (2013). However, at this stage, it is only a support aid in calculating the corresponding new speciation ratio when the Hg_{anthr} emissions are reduced for a specific (set of) macro-sector(s). The possibility of applying one of a set of available BAT(s) to reduce Hg_{anthr} emissions for each macro-sector will be introduced in a future development step, along with the incurred economic and social costs, in order

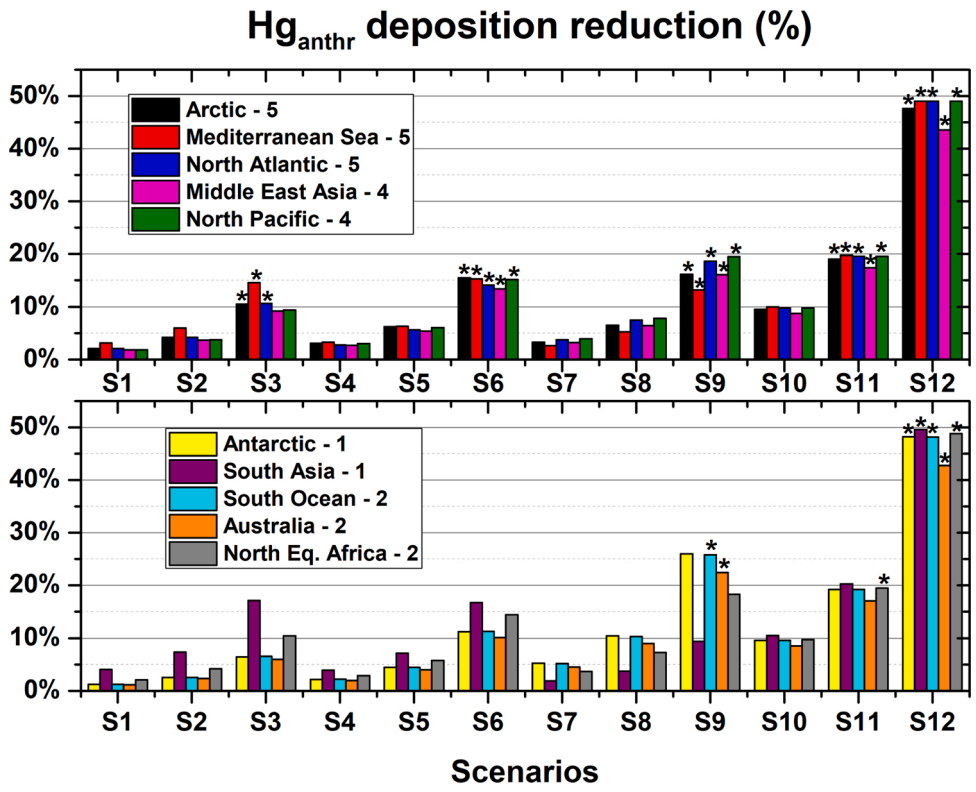

Fig. 7. Receptors that benefit the most (upper panel) and the least (lower panel), in terms of the number of scenarios (reported in the legend) where the Hg_{anth} short-term deposition reduction as calculated by HERMES is significant. The asterisks above the bars indicate the significance of the Hg_{anth} short-term deposition reduction.

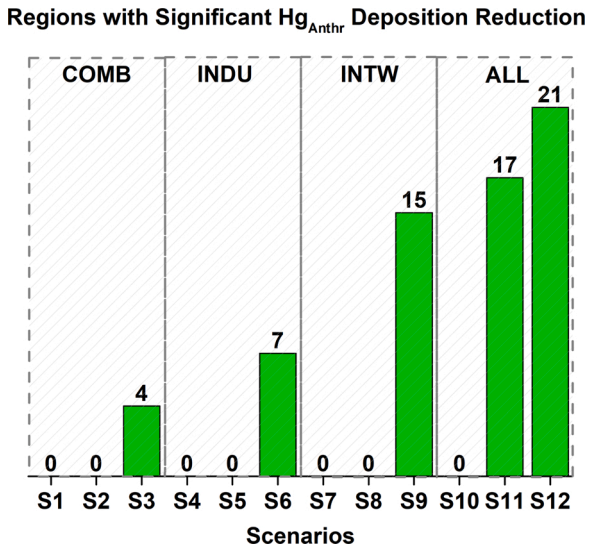

Fig. 8. Numbers of receptors (out of a total of 21) where the Hg_{anth} short-term deposition reduction calculated by HERMES is significant, for each of the scenarios.

that the ratio of environmental benefits to economic costs may be evaluated.

It should be noted that the significance of a policy scenario regarding the Hg_{anthr} deposition over a receptor region, as calculated by HERMES, is evaluated by comparing the newly calculated value with confidence intervals (at 95% level) estimated for the current Hg_{anthr} deposition, considering an ensemble of runs covering a reasonable range of possible sources of uncertainty, as described in (De Simone et al., 2017b), and with the limitations detailed in (De Simone et al., 2020).

In this version, the estimated confidence intervals (at 95% level) associated with the current Business as Usual BGCM variable is calculated for different initial conditions, in particular by running the BGCM also for lower and upper limit of confidence intervals (at 95% level) of the deposition of Hg_{anthr} over oceans, and calculated by CTM (see De Simone et al. (2017b).

As a natural, further evolution of the GOS^{4}M-KH, the inclusion of a BIOTA model will permit to calculate the impact of Hg_{anthr} emission perturbations on Hg concentration in biota, following one of the approaches proposed in literature Schaefer et al. (2020) and Zhang et al. (2020), or a newly developed method. This element will close the loop from emissions to marine biota, since human exposure to Hg occurs primarily via the consumption of food containing methylmercury (MeHg), the toxic form of Hg (Bellanger et al., 2013). Currently, a non-tested *BIOTA output* widget is present in GOS^{4}M-KH, as illustrated in Appendix A.1. However, at the moment of submission of this manuscript this widget is for illustrative purpose only.

Both the existing BGCM and the forthcoming biota model will be modifiable to explicitly account for climate changes in future versions. Indeed, the final exposure to MeHg depends on a set of interlinking physical, biological, chemical and geological processes including release of emission, transport and chemical transformation into atmosphere, deposition, air-sea exchange, air-land exchange, chemical transformation (in particular Hg methylation) in oceanic compartments, food web transfers, and human food intake, that are all influenced by climate change, land-use, ocean circulation, and ecosystem functions (Giang and Selin, 2015; Schartup et al., 2019; Schaefer et al., 2020).

Additional Hg_{anthr} emission inventories, including AMAP, EDGAR tox v1 and 2 (Muntean et al., 2014, 2018), WHET (Zhang et al., 2016b), and STREETS (Streets et al., 2009; Corbitt et al., 2011), is scheduled to be shortly included in HERMES, as well as the results of other models, such as GEOS-Chem (Horowitz et al., 2017), either explicitly or integrated in the uncertainty assessment. Therefore, the next versions of the GOS^{4}M-KH will be more robust in representing the uncertainty arising

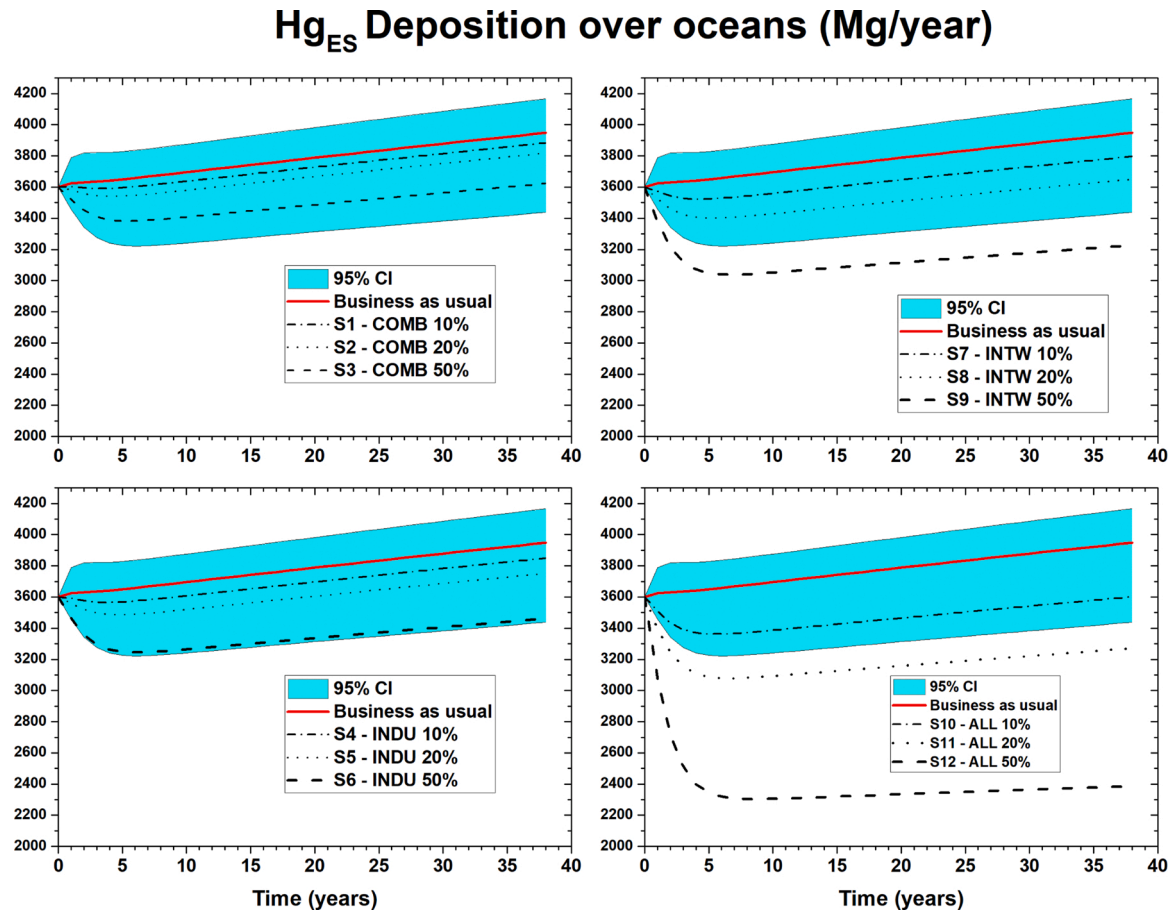

Fig. 9. Hg_{ES} deposition over the oceans from the BCGM model for the different scenarios compared with the Business as Usual.

from using emission inventories and CTMs other than currently supported, as well as in considering the most recent Hg_{anthr} emission estimates.

5. Conclusions

In this study we demonstrated the capabilities of the GOS^{4}M-KH to analyse Hg_{anthr} selected anthropogenic emission reduction scenarios in supporting interested parties to identify cost-effective strategies that could be more suitable for a given country or region to achieve the targets of the Minamata Convention on Mercury. The dashboard back-end is designed to house different computing modules, which are arranged in such a way to realise a workflow addressed to study the overall path of Hg, from its atmospheric releases from anthropogenic activities to its final end points. Currently, the web application includes two computing modules: HERMES, a Hg-CTM emulator (De Simone et al., 2020), built on the ECHMERIT runs (Jung et al., 2009; De Simone et al., 2017b), with the purpose of calculating the short-term fate of Hg_{anthr} emissions over receptor regions, and a Biogeochemical Model, adapted from (Selin, 2014), to investigate the long-term effect on Hg_{ES} cycling. These two computing modules are designed to be very efficient regarding computing time in order to give a real-time experience, with no lags, to the final users. The dashboard interface is designed with a set of different widgets arranged to be consistent with the workflow of computing modules of the back-end, providing the final users with the possibility to follow the entire process in an intuitive and easy experience. Therefore, the GOS^{4}M-KH provides the possibility to exploit complex numerical tools available for modelling the Hg cycle in the atmosphere and other compartments of the ES for users with no specific formation or training.

The GOS^{4}M-KH's purpose is to be an important link between the scientific community and policy makers and other stakeholders to share the latest scientific discoveries to decision makers. In this regard the entire web dashboard was designed to be modular to include different computing modules from other research groups or updated versions thereof, allowing for new kinds of analysis to be included, or for new model or simulation ensembles to be accounted for, either explicitly or in the uncertainty analysis.

From both a scientific and a policy point of view, the set of policy Hg_{anthr} emission reduction scenarios described above, demonstrates that only internationally coordinated actions on multiple sectors would have the ability to attain meaningful effects on the environmental pressure of Hg over either the short- and long-term.

A final consideration pertains to the overall user experience and efficiency of the GOS^{4}M-KH compared to that provided by traditional modelling tools. In particular, the analysis of each of the 12 scenarios assessed in this study would have required a period from days to weeks, to prepare inputs, run the models and then collect, analyse, and summarise the results. Using GOS^{4}M-KH, this task was performed in seconds!

Authors' contribution

The research has been conceived with the joint contribution of all Authors. In particular conceptualisation, Francesco De Simone, Nicola Pirrone, Sergio Cinnirella; methodology, Francesco De Simone, Ian M. Hedgecock; software, Francesco De Simone, Francesco D'Amore; resources, Francesca Sprovieri, Nicola Pirrone; validation and investigation, Francesco De Simone, Francesco Carbone, Francesco D'Amore, Mariantonia Bencardino; supervision, Nicola Pirrone, Francesca

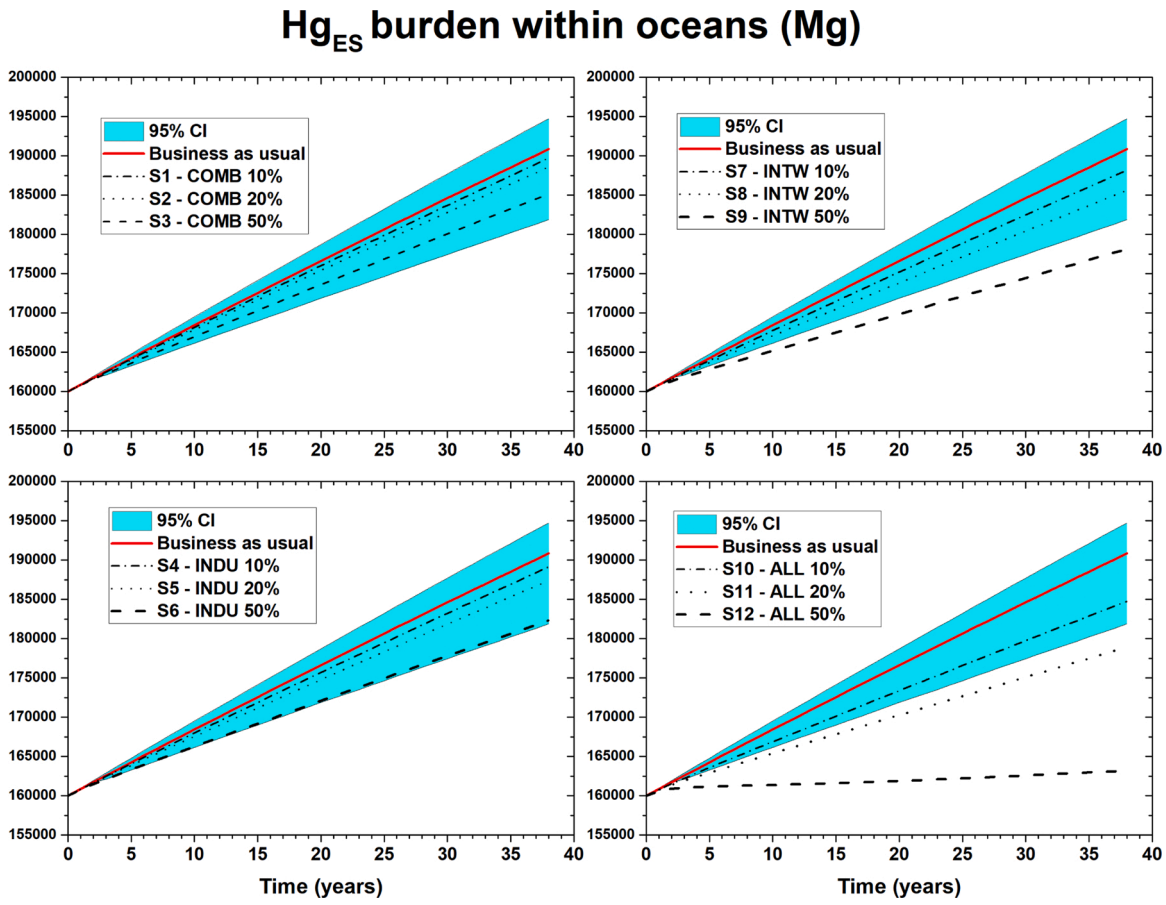

Fig. 10. Hg_{ES} burden within intermediate ocean layer from the BGM model for different scenarios compared to Business as Usual.

Sprovieri, Ian M. Hedgecock and Sergio Cinnirella; funding acquisition, Nicola Pirrone; writing–original draft preparation, Francesco De Simone, Francesco D'Amore; writing–review and editing, Francesco De Simone, Nicola Pirrone, Francesca Sprovieri, Ian M. Hedgecock and Sergio Cinnirella;

Declaration of Competing Interest

The authors report no declarations of interest.

Acknowledgements

The authors would like to acknowledge the contribution received from EU-H2020 projects which includes ERA-PLANET (Grant Agreement: 689443), through the funded project iGOSP, and E-Shape (Grant Agreement: 820852). The contents and appearance of the web platform are under a continual process of development, thus the GOS4M Knowledge Hub in future may appear slightly different from the screenshots presented in this article.

Appendix A. Supplementary data

Supplementary data associated with this article can be found, in the online version, at https://doi.org/10.1016/j.envsci.2021.06.021.

References

AMAP/UNEP, 2013. Technical Background Report for the Global Mercury Assessment 2013. Technical Report. Arctic Monitoring and Assessment Programme, Oslo, Norway/UNEP Chemicals Branch, Geneva, Switzerland. http://www.unep.org/hazardoussubstances/Mercury/Informationmaterials/ReportsandPublications/tabid/3593/Default.aspx.

Amos, H.M., Jacob, D.J., Holmes, C., Fisher, J.A., Wang, Q., Yantosca, R.M., Corbitt, E.S., Galarneau, E., Rutter, A., Gustin, M., et al., 2012. Gas-particle partitioning of atmospheric hg (ii) and its effect on global mercury deposition. Atmos. Chem. Phys. 12, 591–603.

Amos, H.M., Jacob, D.J., Kocman, D., Horowitz, H.M., Zhang, Y., Dutkiewicz, S., Horvat, M., Corbitt, E.S., Krabbenhoft, D.P., Sunderland, E.M., 2014. Global biogeochemical implications of mercury discharges from rivers and sediment burial. Environ. Sci. Technol. 48, 9514–9522.

Amos, H.M., Jacob, D.J., Streets, D.G., Sunderland, E.M., 2013. Legacy impacts of all-time anthropogenic emissions on the global mercury cycle. Glob. Biogeochem. Cycles 27, 410–421.

Bellanger, M., Pichery, C., Aerts, D., Berglund, M., Castaño, A., Čejchanová, M., Crettaz, P., Davidson, F., Esteban, M., Fischer, M.E., et al., 2013. Economic benefits of methylmercury exposure control in Europe: monetary value of neurotoxicity prevention. Environ. Health 12, 1–10.

Chen, L., Liang, S., Liu, M., Yi, Y., Mi, Z., Zhang, Y., Li, Y., Qi, J., Meng, J., Tang, X., et al., 2019. Trans-provincial health impacts of atmospheric mercury emissions in China. Nat. Commun. 10, 1–12.

Corbitt, E.S., Jacob, D.J., Holmes, C.D., Streets, D.G., Sunderland, E.M., 2011. Global source-receptor relationships for mercury deposition under present-day and 2050 emissions scenarios. Environ. Sci. Technol. 45, 10477–10484.

D'Amore, F., Cinnirella, S., Pirrone, N., 2012. Ict methodologies and spatial data infrastructure for air quality information management. IEEE J. Sel. Top. Appl. Earth Observ. Rem. Sens. 5, 1761–1771.

Dastoor, A., Ryzhkov, A., Durnford, D., Lehnherr, I., Steffen, A., Morrison, H., 2015. Atmospheric mercury in the Canadian arctic. Part II: insight from modeling. Sci. Total Environ. 509, 16–27.

De Simone, F., Gencarelli, C., Hedgecock, I., Pirrone, N., 2014. Global atmospheric cycle of mercury: a model study on the impact of oxidation mechanisms. Environ. Sci. Poll. Res. 21, 4110–4123.

De Simone, F., Cinnirella, S., Gencarelli, C.N., Yang, X., Hedgecock, I.M., Pirrone, N., 2015. Model study of global mercury deposition from biomass burning. Environ. Sci. Technol. 49, 6712–6721.

De Simone, F., Gencarelli, C.N., Hedgecock, I.M., Pirrone, N., 2016. A modeling comparison of mercury deposition from current anthropogenic mercury emission inventories. Environ. Sci. Technol. 50, 5154–5162.

De Simone, F., Artaxo, P., Bencardino, M., Cinnirella, S., Carbone, F., D'Amore, F., Dommergue, A., Feng, X.B., Gencarelli, C.N., Hedgecock, I.M., Landis, M.S., Sprovieri, F., Suzuki, N., Wängberg, I., Pirrone, N., 2017a. Particulate-phase mercury emissions from biomass burning and impact on resulting deposition: a modelling

assessment. Atmos. Chem. Phys. 17, 1881–1899. https://doi.org/10.5194/acp-17-1881-2017.

De Simone, F., Hedgecock, I.M., Carbone, F., Cinnirella, S., Sprovieri, F., Pirrone, N., 2017b. Estimating uncertainty in global mercury emission source and deposition receptor relationships. Atmosphere 8. https://doi.org/10.3390/atmos8120236.

De Simone, F., D'Amore, F., Marasco, F., Carbone, F., Bencardino, M., Hedgecock, I.M., Cinnirella, S., Sprovieri, F., Pirrone, N., 2020. A chemical transport model emulator for the interactive evaluation of mercury emission reduction scenarios. Atmosphere 11, 878.

Durnford, D., Dastoor, A., Ryzhkov, A., Poissant, L., Pilote, M., Figueras-Nieto, D., 2012. How relevant is the deposition of mercury onto snowpacks? Part 2: a modeling study. Atmos. Chem. Phys. 12, 9251–9274.

Fraser, A., Dastoor, A., Ryjkov, A., 2018. How important is biomass burning in Canada to mercury contamination? Atmos. Chem. Phys. 18, 7263–7286. https://doi.org/10.5194/acp-18-7263-2018.

Giang, A., Selin, N.E., 2015. Benefits of mercury controls for the United States. Proc. Natl. Acad. Sci. U.S.A. https://doi.org/10.1073/pnas.1514395113.

Holmes, C.D., Jacob, D.J., Corbitt, E.S., Mao, J., Yang, X., Talbot, R., Slemr, F., 2010. Global atmospheric model for mercury including oxidation by bromine atoms. Atmos. Chem. Phys. 10, 12037–12057.

Horowitz, H.M., Jacob, D.J., Zhang, Y., Dibble, T.S., Slemr, F., Amos, H.M., Schmidt, J. A., Corbitt, E.S., Marais, E.A., Sunderland, E.M., 2017. A new mechanism for atmospheric mercury redox chemistry: implications for the global mercury budget. Atmos. Chem. Phys. 17, 6353–6371.

Jung, G., Hedgecock, I.M., Pirrone, N., 2009. ECHMERIT v1.0 – a new global fully coupled mercury-chemistry and transport model. Geosci. Model Dev. 2, 175–195.

Kawai, T., Sakurai, T., Suzuki, N., 2020. Application of a new dynamic 3-d model to investigate human impacts on the fate of mercury in the global ocean. Environ. Modell. Softw. 124, 104599. https://doi.org/10.1016/j.envsoft.2019.104599.

Kos, G., Ryzhkov, A., Dastoor, A., Narayan, J., Steffen, A., Ariya, P., Zhang, L., 2013. Evaluation of discrepancy between measured and modelled oxidized mercury species. Atmos. Chem. Phys. 13, 4839–4863.

Muntean, M., Janssens-Maenhout, G., Song, S., Giang, A., Selin, N.E., Zhong, H., Zhao, Y., Olivier, J.G., Guizzardi, D., Crippa, M., Schaaf, E., Dentener, F., 2018. Evaluating edgarv4.tox2 speciated mercury emissions ex-post scenarios and their impacts on modelled global and regional wet deposition patterns. Atmos. Environ. 184, 56–68. https://doi.org/10.1016/j.atmosenv.2018.04.017.

Muntean, M., Janssens-Maenhout, G., Song, S., Selin, N.E., Olivier, J.G., Guizzardi, D., Maas, R., Dentener, F., 2014. Trend analysis from 1970 to 2008 and model evaluation of {EDGARv4} global gridded anthropogenic mercury emissions. Sci. Total Environ. 494–495, 337–350.

Saiz-Lopez, A., Sitkiewicz, S.P., Roca-Sanjuán, D., Oliva-Enrich, J.M., Dávalos, J.Z., Notario, R., Jiskra, M., Xu, Y., Wang, F., Thackray, C.P., et al., 2018. Photoreduction of gaseous oxidized mercury changes global atmospheric mercury speciation, transport and deposition. Nat. Commun. 9, 1–9.

Schaefer, K., Elshorbany, Y., Jafarov, E., Schuster, P.F., Striegl, R.G., Wickland, K.P., Sunderland, E.M., 2020. Potential impacts of mercury released from thawing permafrost. Nat. Commun. 11, 1–6.

Schartup, A.T., Thackray, C.P., Qureshi, A., Dassuncao, C., Gillespie, K., Hanke, A., Sunderland, E.M., 2019. Climate change and overfishing increase neurotoxicant in marine predators. Nature 572, 648–650.

Selin, N.E., 2014. Global change and mercury cycling: challenges for implementing a global mercury treaty. Environ. Toxicol. Chem. 33, 1202–1210. https://doi.org/10.1002/etc.2374.

Song, S., Selin, N.E., Soerensen, A.L., Angot, H., Artz, R., Brooks, S., Brunke, E.G., Conley, G., Dommergue, A., Ebinghaus, R., et al., 2015. Top-down constraints on atmospheric mercury emissions and implications for global biogeochemical cycling. Atmos. Chem. Phys. 15, 7103–7125.

Streets, D.G., Zhang, Q., Wu, Y., 2009. Projections of global mercury emissions in 2050. Environ. Sci. Technol. 43, 2983–2988.

Talia, D., 2015. Making knowledge discovery services scalable on clouds for big data mining. 2015 2nd IEEE International Conference on Spatial Data Mining and Geographical Knowledge Services (ICSDM) 1–4. https://doi.org/10.1109/ICSDM.2015.7298015.

Travnikov, O., Angot, H., Artaxo, P., Bencardino, M., Bieser, J., D'Amore, F., Dastoor, A., De Simone, F., Diéguez, M.D.C., Dommergue, A., Ebinghaus, R., Feng, X.B., Gencarelli, C.N., Hedgecock, I.M., Magand, O., Martin, L., Matthias, V., Mashyanov, N., Pirrone, N., Ramachandran, R., Read, K.A., Ryjkov, A., Selin, N.E., Sena, F., Song, S., Sprovieri, F., Wip, D., Wängberg, I., Yang, X., 2017. Multi-model study of mercury dispersion in the atmosphere: atmospheric processes and model evaluation. Atmos. Chem. Phys. 17, 5271–5295. https://doi.org/10.5194/acp-17-5271-2017.

Travnikov, O., Ilyin, I., 2009. The emep/msc-e mercury modeling system. Mercury Fate and Transport in the Global Atmosphere 571–587.

Travnikov, O., Jonson, J., Andersen, A., Gauss, M., Gusev, A., Rozovskaya, O., Simpson, D., Sokovyh, V., Valiyaveetil, S., Wind, P., 2009. Development of the EMEP Global Modelling Framework: Progress Report. Technical Report. EMEP/MSC-E Technical Report 7/2009. Meteorological Synthesizing Centre-East.

UN-Environment, 2019. Update on Matters Related to the Global Environment Facility. http://www.mercuryconvention.org/Portals/11/documents/meetings/COP3/English/UNEP-MC-COP-3-9-GEF.English.pdf.

Zhang, H., Holmes, C., Wu, S., 2016a. Impacts of changes in climate, land use and land cover on atmospheric mercury. Atmos. Environ. 141, 230–244.

Zhang, Y., Horowitz, H., Wang, J., Xie, Z., Kuss, J., Soerensen, A.L., 2019. A coupled global atmosphere-ocean model for air-sea exchange of mercury: insights into wet deposition and atmospheric redox chemistry. Environ. Sci. Technol. 53, 5052–5061. https://doi.org/10.1021/acs.est.8b06205.

Zhang, Y., Jacob, D.J., Horowitz, H.M., Chen, L., Amos, H.M., Krabbenhoft, D.P., Slemr, F., Louis, V.L.S., Sunderland, E.M., 2016b. Observed decrease in atmospheric mercury explained by global decline in anthropogenic emissions. Proc. Natl. Acad. Sci. U.S.A. 113, 526–531.

Zhang, Y., Soerensen, A.L., Schartup, A.T., Sunderland, E.M., 2020. A global model for methylmercury formation and uptake at the base of marine food webs. Glob. Biogeochem. Cycles 34 e2019GB006348.

Zhou, J., Obrist, D., Dastoor, A., Jiskra, M., Ryjkov, A., 2021. Vegetation uptake of mercury and impacts on global cycling. Nat. Rev. Earth Environ. 1–16.